

K. Viscoplastic Twinning in an Ultrafine TiAl/Ti₃Al Laminate Composite

Luke Hsiung

Chemistry and Materials Science Directorate

Lawrence Livermore National Laboratory

L-352, P.O. Box 808

Livermore, CA 9455-9900

(925)-424-3125; fax: (925) 424-3815; email: hsiung1@llnl.gov

DOE Technology Development Area Specialist: James J. Eberhardt

(202) 586-9837; fax: (202) 586-1600; e-mail: james.eberhardt@ee.doe.gov

ORNL Technical Advisor: D. Ray Johnson

(865) 576-6832; fax: (865) 574-6098; e-mail: johnsondr@ornl.gov

Contractor: Oak Ridge National Laboratory, Oak Ridge, Tennessee

Contract No.: DE-AC05-00OR22725

Subcontractor: Lawrence Livermore National Laboratory

Objectives

- Exploit thermomechanical-processing techniques to fabricate TiAl/Ti₃Al nanolaminate composites with lamella widths down to nanometer length scales.
- Characterize microstructure and elevated-temperature creep resistance of the nanolaminate composites.
- Investigate the fundamental interrelationships among microstructures, alloying additions, and mechanical properties of the nanolaminate composites to achieve the desired properties of the composites for high-temperature structural applications.

Approach

- Employ in-situ laminate composites with nominal compositions of Ti-47Al-2Cr-2Nb, Ti-46Al-3Nb-1W-0.1B, and Ti-46Al-3Nb-2W-0.1B (at. %). The in-situ laminate composites were fabricated at Oak Ridge National Laboratory (ORNL) by hot extrusion of cast alloys at 1350°C.
- Conduct creep tests in a dead-load creep machine with a lever arm ratio of 16:1. Tests were performed in air in a split furnace with three zones at 760 and 815°C.
- Examine the microstructures of creep-deformed samples using a JEOL-200CX transmission electron microscope (TEM).

Introduction

Two-phase [TiAl (γ -L10) and Ti₃Al (α 2-DO19)] fully lamellar TiAl alloys have recently attracted much attention because of their low density ($\rho = 3.9$ g/cc), high specific strength, adequate oxidation resistance, and good combination of ambient-temperature and elevated-temperature mechanical properties, which are of interest for aerospace and

transportation applications such as high-temperature components in turbine and combustion engines. Through alloy design and microstructural refinement, significant progress has been made recently to improve both room-temperature ductility/toughness and high-temperature creep resistance of the material.¹⁻⁵ One of the interesting deformation substructures of the laminate material with an ultrafine microstructure is the formation of

high-density twin lamellae with the widths in the sub-micrometer or nanometer length scale.⁵ The most unique characteristic of the twinning phenomenon observed from the TiAl/Ti₃Al laminate material is that it can even take place at elevated temperatures under loading conditions such that the steady creep rate is as low as 10^{-7} s^{-1} and with a stress level much lower than its yield strength. This viscoplastic twinning phenomenon is different from the twinning phenomenon that commonly occurs in conventional metals and alloys deformed under low-temperature and/or high strain-rate conditions. It has been reported previously that the occurrence of $\{111\}\langle 112 \rangle$ -type twinning in the TiAl/Ti₃Al laminate material is intimately related to the dissociation of dislocations in laminate interfaces and the homogeneous glide of $1/6 \langle 11\bar{2} \rangle$ twinning dislocations in the $\{111\}$ planes of γ lamellae.⁶ Results obtained from more rigorous TEM analyses are reported here in order to further elucidate the underlying mechanisms for the occurrence of viscoplastic twinning in the TiAl/Ti₃Al laminate material.

Approach

The ultrafine two-phase [TiAl-(γ)/Ti₃Al-(α_2)] lamellar alloy was fabricated by a powder metallurgy process, which involves hot extrusion of gas-atomized titanium aluminide powder with a nominal composition of Ti-47Al-2Cr-2Nb (at. %) at 1400°C. After extrusion, the material was stress relieved at 900°C in a vacuum ($\sim 10^{-4}$ Pa) for 2 h. Creep tests were conducted at 760°C in a dead-load creep machine with a lever arm ratio of 16:1. Detailed information regarding the creep experiment and experimental data were reported elsewhere.⁵ For the current study, the deformation substructure of a specimen tested at 138 MPa with a steady creep-rate of $2.0 \times 10^{-9} \text{ s}^{-1}$, and that of a specimen tested at 518 MPa with a steady creep-rate of $2.5 \times 10^{-7} \text{ s}^{-1}$ were examined. TEM foils were prepared by twin-jet electropolishing in a solution of 60 vol % methanol, 35 vol % butyl alcohol and 5 vol % perchloric acid at ~ 15 V and -30°C . The microstructures of both as-fabricated material and tested samples were examined using a JEOL-200CX TEM equipped with a double-tilt goniometer stage. Images of microstructures were recorded using high-resolution lattice imaging techniques and weak-

beam dark field (WBDF) imaging techniques under g ($3g$) two-beam diffraction conditions with the deviation factor $\omega (= \xi_g s) > \sim 1$, where ξ_g is the extinction distance and s is the deviation distance from the exact Bragg position. The g - b invisibility criteria used for determining the Burgers vector of Shockley partials are described as follows:⁷ (a) invisible if $g \cdot b = 0$ or $\pm 1/3$; (b) invisible if $g \cdot b = -2/3$ but visible if $g \cdot b = +2/3$ provided the deviation factor $\omega > \sim 1$; (c) invisible if $g \cdot b = +4/3$ but visible if $g \cdot b = -4/3$, provided the deviation factor $\omega > \sim 1$.

Results

Movement and Pileup of Interfacial Dislocations

The results of an in-situ TEM experiment that directly observed cooperative movement of interfacial dislocations in a TiAl/Ti₃Al laminate sample under room-temperature straining conditions have been reported previously.⁸ Figure 1 is a typical example showing that the interfacial dislocations can be blocked by impinged lattice dislocations during their movement along a laminate interface. Here, a dislocation network formed by the reaction between impinged lattice dislocations and interfacial dislocations can be readily seen in a γ/α_2 interface. Figure 2 shows the results of an in-situ TEM experiment, which evidence the motion and pile-up

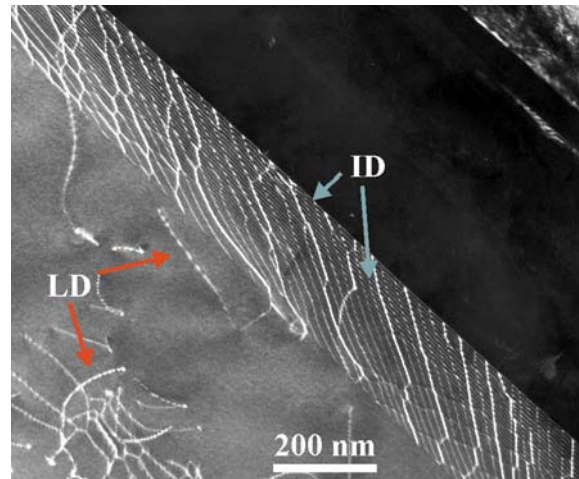


Figure 1. A WBDF TEM image shows that the movement of interfacial dislocations is hampered because of the formation of dislocation networks as a result of the reaction between impinged lattice dislocations (LD) and interfacial dislocations (ID).

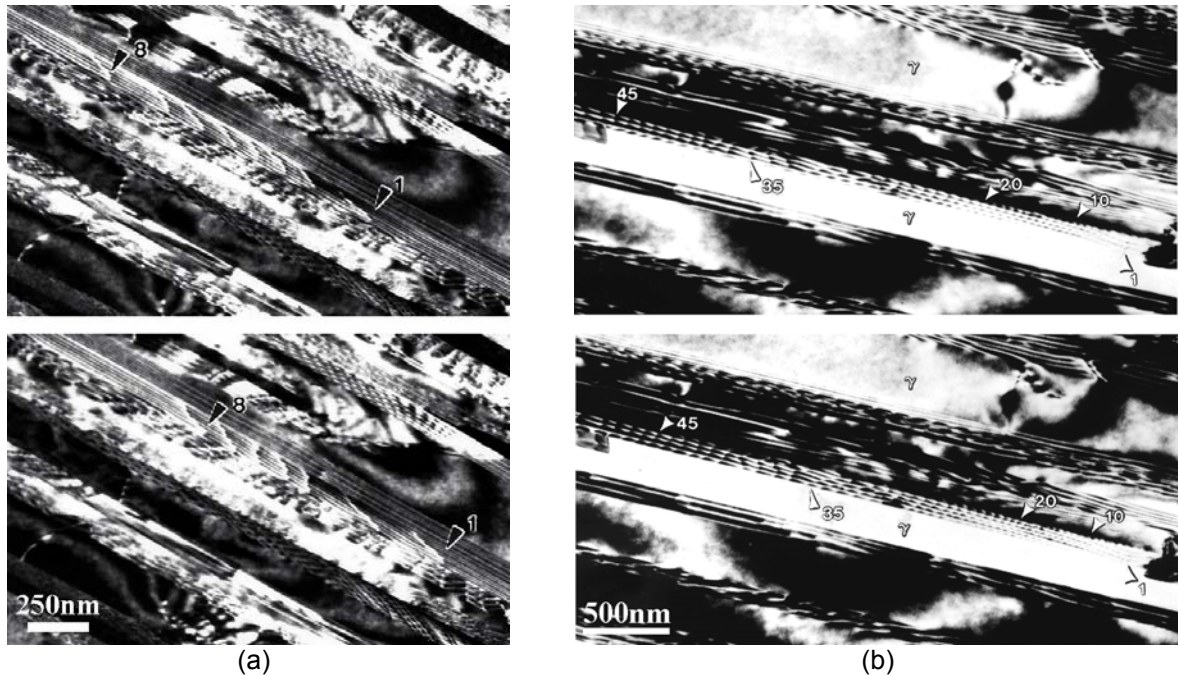


Figure 2. Consecutive in-situ TEM images show (a) the movement of an interfacial dislocation array in a laminate interface (time span: 30 s), and (b) the movement and pile-up of interfacial dislocations in a laminate interface adjacent to the tip of an α_2 fragment (time span: 30 s).

of interfacial dislocations during electron-beam heating of a thin foil (prepared from a sample pre-crept at 760°C and 138 MPa) that contains residual stress. The original idea of this experiment assumes that the relaxation of residual stress can result in the motion of interfacial dislocations. Since the purpose of the study is only to demonstrate the interfacial dislocation motion, the amount of temperature increase by beam heating is not a major concern. It is also noted that local heating can be achieved when an electron beam is focused on a small spot the size of several micron meters. Figure 2(a) shows the cooperative motion of a dislocation array of eight interfacial dislocations on a laminate interface. It is interesting to note that the motion of each dislocation was in a viscous drifting or pinning/unpinning fashion, and each of them has a different drifting velocity. Here, after beam focusing (heating) for 30 s, the No. 1 leading dislocation of the array moved about 375 nm, and the No. 8 trailing dislocation moved about 425 nm. This suggests that each dislocation has different mobility as a result of the solute-dragging effect. Figure 2(b) shows the motion of interfacial dislocations within a dislocation pileup on a laminate interface. Here, the head of the dislocation pileup is at the tip of a

faulted α_2 -lamella adjacent to the No. 1 dislocation. Notice that the dislocation spacing increases with increasing distance from the head of the pile-up, and those dislocations close to the head of the pile-up moved slower than those distant from the head. For instance, the No. 10 and No. 20 dislocations moved about 170 nm, and the No. 35 and No. 45 dislocations moved about 250 nm after beam focusing (heating) for 30 s. That is, during beam heating, dislocations in the pile-up start to squeeze, which causes the increase of dislocation density within the pile-up.

These in-situ observations of interfacial dislocation motion and pile-up are rationalized below. Since the thin foil contains residual stress, each dislocation starts to move under a heating condition with a velocity $v = MF$, where v is the (drift) velocity of dislocation, M is the mobility of dislocation, and F is the effective force acting on the dislocation. An explicit expression for the dislocation mobility M limited by solute drag can be found in Ref. 9:

$$M = \frac{D_s \Omega}{\beta b^2 C_0 k T} ,$$

where β is a constant, b is the length of Burgers vector, C_0 is the solute concentration, D_s is the solute diffusion coefficient, and Ω is the atomic volume of the solute. The effective force (F) acting on the i -th dislocation in a dislocation array or pile-up can be expressed as

$$F = \tau b - \frac{\mu b^2}{2\pi(I-\nu)} \sum_{\substack{j=0 \\ j \neq i}}^n \frac{I}{x_i - x_j},^{10}$$

where the term

$$\frac{\mu b^2}{2\pi(I-\nu)} \sum_{\substack{j=0 \\ j \neq i}}^n \frac{I}{x_i - x_j}$$

represents the sum of internal forces acting on the i -th dislocation by the other dislocations of the pile-up; $x_i - x_j$ represents the distance between the i -th and j -th dislocations. Accordingly, ν increases as a result of the increase of dislocation mobility as temperature (T) increases during beam heating, and ν diminishes as temperature decreases to an ambient temperature. The velocity of dislocations close to the head of the pile-up becomes slower, indicating that the internal stress acting on the dislocations increases as the dislocations move closer to the head, and therefore reducing the effective force (F) acting on the dislocations.

Viscoplastic Deformation Twinning

When an alloy sample was creep-deformed at 760°C with a constant applied stress of 518 MPa under a strain rate of $3 \times 10^{-7} \text{ s}^{-1}$, a deformation substructure associated with deformation twins was developed within γ lamellae. Typical $(\bar{1}11)$ [211]-type twin lamellae formed within γ lamellae are shown in Figure 3. Notice that one of the twin lamellae in Figure 3(a) (labeled by an arrow) was still growing toward another interface. Similar features were also observed elsewhere in the same sample. This suggests that the laminate interface is the major source for the occurrence of viscoplastic deformation twinning. The viscoplastic twinning phenomenon can be viewed as a relaxation process to relieve the local stress concentration caused by the pile-up of interfacial dislocations. The effective stress (τ_e) at the head of the pile-up of n dislocations

can be evaluated by $\tau_e = n\tau I$ (Ref. 11), where τ_i is the resolved shear stress acting on the interface. To relieve the stress concentration, deformation twinning in γ layers is therefore taking place by a dislocation reaction based upon a stair-rod cross-slip mechanism, as schematically illustrated in Figure 3(b). For the formation of a $(\bar{1}11)$ -type twin lamella, the corresponding dislocation reaction is $1/6[\bar{1}2\bar{1}](111)[\mathbf{b}_1] \rightarrow 1/6[011](100)[\mathbf{b}_2] + 1/6[\bar{1}1\bar{2}](\bar{1}11)[\mathbf{b}_3]$. The $(\bar{1}11)$ -type twin is accordingly formed within γ lamella by successively dissociating the $[\mathbf{b}_1]$ interfacial dislocations in the pile-up and emitting the $[\mathbf{b}_3]$ twinning dislocations into the $(\bar{1}11)$ γ plane and leaving the $[\mathbf{b}_2]$ stair-rod dislocations in the $(100)\gamma$ plane. Figures 3(c) and 3(d) show the edge-on views of the $(\bar{1}11)$ -type twin lamellae, in which their widths were measured as varying between 3 and 20 nm.

The formation of $[\mathbf{b}_2]$ stair-rod dislocations at the intersections between twin and α_2 lamellae is evidenced in Figures 4(a) and 4(b), in which the array of $1/6[011]$ stair-rod dislocations becomes invisible [Figure 4(a)] or visible [Figure 4(b)] when a reflection vector (g) 200 or 021 is used for imaging. It is noted that the individual stair-rod dislocation is not resolvable because of a narrow distance (0.25 nm) between two stair-rod dislocations. The formation of $[\mathbf{b}_3]$ twinning dislocations for the $(\bar{1}11)$ -type twin lamella is evidenced in Figures 4(c) and 4(d), in which the array of $1/6[112]$ twinning dislocations becomes visible [Figure 4(c)] or invisible [Figure 4(d)] when a reflection vector of 111 or $\bar{2}02$ is used for imaging. The significance of the proposed mechanism is to reveal that there are several barriers to be overcome in order to activate the twinning reaction. These barriers include (1) the repulsive force between the interfacial (Shockley) and stair-rod dislocations, (2) the increase of line energy due to the dislocation dissociation, and (3) the increase of interfacial energy due to the formation of twin faults. Among which the repulsive force (F) between the interfacial (Shockley) and stair-rod dislocations is considered to be the rate-limiting process. That is, a critical stress (τ_c) is required to activate for the twinning reaction, i.e., to activate the dissociation reaction for twinning. Assuming an isotropic elasticity, the critical stress (τ_c) can be approximately evaluated as

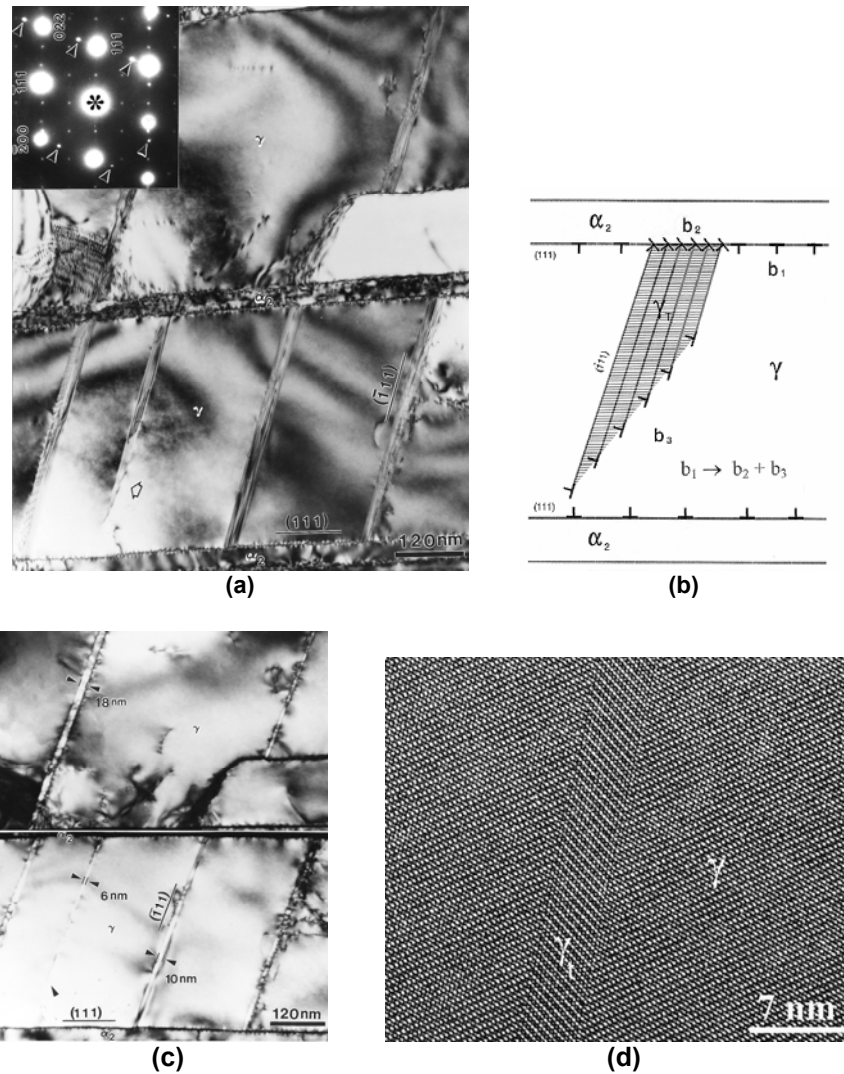


Figure 3. A dark-field TEM image shows several ($\bar{1}11$) type twin lamellae formed within a γ lamella (a); a schematic illustration of the nucleation of a ($\bar{1}11$) type twin lamella (γ_t) from a γ/α_2 interface (b), where b_1 , b_2 , and b_3 denote the interfacial, stair-rod, and twinning dislocations, respectively; and edge-on views of twin lamellae show the widths of the ($\bar{1}11$)-type twin lamellae (c) and (d).

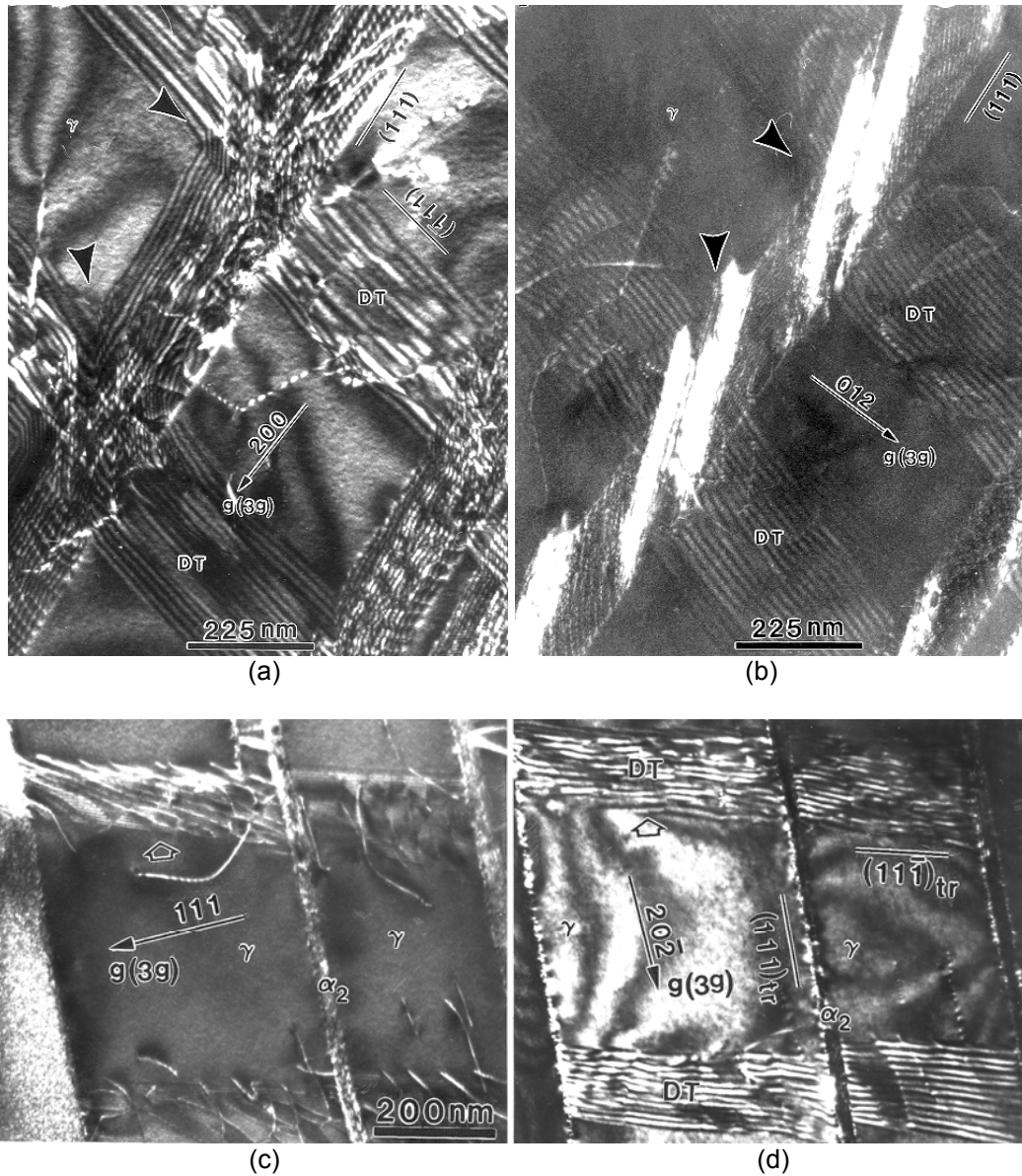


Figure 4. WBDF TEM images show the g-b contrast visibility analyses for the arrays of $[b_2]$ $1/6[011]$ stair-rod dislocations formed at the intersections (indicated by arrows) between the $(\bar{1}11)$ -type deformation twins (DT) and α_2 lamellae: (a) Z (zone axis) $\approx [0\bar{1}2]$, $g = 200$, $g \cdot b = 0$ (invisible), (b) $Z \approx [0\bar{1}2]$, $g = 021$, $g \cdot b = 1/2$ (visible); and the analyses for the arrays of $[b_3]$ $1/6[112]$ twinning dislocations of the $(11\bar{1})$ -type deformation twins: (c) $Z \approx [\bar{1}2\bar{1}]$, $g = 111$, $g \cdot b = 2/3$, (visible), and (d) $Z \approx [\bar{1}2\bar{1}]$, $g = 20\bar{2}$, $g \cdot b = 1/3$ (invisible).

$\tau_c b_1 = F \approx \eta \mu b_1 b_2 \cos \theta / 2\pi r$, where $\eta = 1$ for screw dislocations and $\eta = 1/(1 - \nu)$ for edge dislocations; ν is Poisson's ratio (~ 0.3); μ is shear modulus (~ 56 GPa at 760°C) (Ref. 12); $b_1 = 0.163$ nm; and $b_2 = 0.094$ nm for Shockley and stair-rod dislocations, respectively; θ ($= 54.4^\circ$) is the angle

between $(\bar{1}11)$ and (100) planes; and r (0.25 nm) is the distance between the two dislocations. The critical stress (τ_c) required for twinning is thus approximately 1.95 GPa for screw dislocations and 2.79 GPa for edge dislocations.

In the case of a low applied stress (138 MPa), the resolved shear stress (τ_i) acting on the interface plane is about 69 MPa (assuming Schmid factor = 0.5), and the number of pile-up dislocations required to create a sufficient stress concentration (i.e., $\tau_e = n\tau_i \geq \tau_c$) for twinning to occur is $n \geq 29$. In the case of a high applied stress (518 MPa), the resolved shear stress acting on the same interface plane is about 259 MPa, and the number of pile-up dislocations required for twinning to occur is $n \geq 8$. Thus the accumulation creep strain required to bring on the viscoplastic twinning is smaller and therefore easier to reach. Besides, the average velocity of dislocations is relatively faster when tested under a high applied stress, since the strain rate is higher, which gives a shorter time to develop a pile-up configuration when tested under high applied stresses. That is, it is more feasible that the viscoplastic twinning will take place when the laminate is creep-deformed under high applied stresses. A recent report on deformation twinning of the same material creep-deformed under different loading conditions has evidenced that the twinning occurred shortly after the creep strain reached 0.67% under a high applied stress (518 MPa), whereas the twinning took place when the creep strain reached ~1.5% under a low applied stress (138 MPa).¹³

Conclusion

The viscoplastic twinning phenomenon, which takes place within an ultrafine TiAl/Ti₃Al laminate composite subjected to an elevated-temperature creep deformation, has been studied. The viscoplastic twinning phenomenon is found to be intimately related to the movement, pile-up, and dissociation of the pre-existing dislocation arrays in laminate interfaces. When the arrays of interfacial dislocation (e.g., $1/6\langle 112 \rangle$ Shockley partials) move along the interfaces, obstacles such as impinged lattice dislocations, and interfacial ledges can impede their movement. The dislocation arrays start piling up behind an obstacle because an individual Shockley partial is energetically unfavorable to undergo cross-slip or climb that otherwise will generate stacking fault on its wake if it moves away from the interface. Thus the arrays of interfacial dislocations can easily be piling up even at elevated temperatures. The viscoplastic twinning within the creep-deformed laminate can accordingly be rationalized as a relaxation process to dissipate the internal stress resulting

from dislocation pile-up. The twinning process involves the dissociation of interfacial dislocation into stair-rod (or residual) and twinning dislocations, i.e., $1/6[\bar{1}2\bar{1}](111) \rightarrow 1/6[011](100) + 1/6[\bar{1}\bar{1}\bar{2}](\bar{1}\bar{1}\bar{1})$ for $(\bar{1}\bar{1}\bar{1})[\bar{1}\bar{1}\bar{2}]$ -type twinning. It is concluded that the dislocation pile-up configuration is a prerequisite to begin the process of deformation twinning, which is more likely to occur under low-temperature and high strain-rate deformation conditions for conventional metals and alloys. The occurrence of time-dependent viscoplastic twinning in the TiAl/Ti₃Al laminate reveals that the dislocation pile-up configuration can be readily formed along laminate interfaces even at elevated temperatures.

References

1. Y-W. Kim and D.M. Dimiduk, *JOM*, **43**(8), 40 (1991).
2. Y-W. Kim, *Acta Metall. Mater.*, **40**, 1121 (1992).
3. C. T. Liu, J. H. Schneibel, P. J. Maziasz, J. L. Wright, and D. S. Easton, *Intermetallics*, **4**, 429 (1996).
4. C. T. Liu, P. J. Maziasz, and J. L. Wright, *Mat. Res. Soc. Symp. Proc.*, **460**, 83 (1997).
5. L. M. Hsiung and T. G. Nieh, *Matls. Sci. & Engrg.*, **A364**, 1 (2004).
6. L. M. Hsiung and T.G. Nieh, *Matls. Sci. & Engrg.*, **A239-240**, 438 (1997).
7. J. W. Edington, *Practical Electron Microscopy in Materials Science*, Van Nostrand Reinhold, New York, 1976.
8. L. M. Hsiung, A. J. Schwartz, and T. G. Nieh, *Intermetallics*, **12**, 727 (2004).
9. E. Arzt, M. F. Ashby, and R. A. Verrall, *Acta Metall.*, **31**, 1977 (1983).
10. J. Weertman, *J. Appl. Phys.*, **28**, 1185 (1957).
11. J. D. Eshelby, F. C. Frank, and F. R. N. Nabarro, *Phil. Mag.*, **42**, 351 (1951).
12. S. C. Huang and J. C. Chesnutt, *Intermetallic Compounds: Principles and Practice 2*, eds. J. H. Westbrook and R. L. Fleischer, John Wiley & Sons, p. 73, 1995.
13. J. G. Wang, L. M. Hsiung, and T. G. Nieh, *Scripta Mater.*, **39**, 957 (1998).

Presentations and Publications

L. M. Hsiung and T. G. Nieh, "In-Situ TEM Study of Interface Sliding and Migration in an

Ultrafine Lamellar Structure,” presented at the 2005 MRS spring meeting.

L. M. Hsiung, “TEM Study of Microstructures in a Creep-Deformed TiAl/Ti₃Al Nanocomposite,” *Heavy Propulsion Materials Program Quarterly Progress Report for October through December*

2004, U.S. Department of Energy, Washington, D.C., 2004.

L. G. Zhou, L. M. Hsiung, and Hanchen Huang, “Nucleation and Propagation of Deformation Twin in Polysynthetically Twinned TiAl,” *Computer Modeling in Engineering and Sciences*, **6**(3) (2004) 245–252.